

PLANT REPRODUCTION

A paternal signal induces endosperm proliferation upon fertilization in *Arabidopsis*

Sara Simonini*, Stefano Bencivenga, Ueli Grossniklaus*

In multicellular organisms, sexual reproduction relies on the formation of highly differentiated cells, the gametes, which await fertilization in a quiescent state. Upon fertilization, the cell cycle resumes. Successful development requires that male and female gametes are in the same phase of the cell cycle. The molecular mechanisms that reinstate cell division in a fertilization-dependent manner are poorly understood in both animals and plants. Using *Arabidopsis*, we show that a sperm-derived signal induces the proliferation of a female gamete, the central cell, precisely upon fertilization. The central cell is arrested in S phase by the activity of the RETINOBLASTOMA RELATED1 (RBR1) protein. Upon fertilization, delivery of the core cell cycle component CYCD7;1 causes RBR1 degradation and thus S phase progression, ensuring the formation of functional endosperm and, consequently, viable seeds.

Sexual reproduction entails specification of the germline and the formation of male and female gametes, which fuse during fertilization (1). In flowering plants, fertilization involves two pairs of gametes that are produced by multicellular gametophytes. The male gametophyte (pollen) germinates to form a pollen tube that transports two sperm cells to the female gametophyte. The latter develops within the ovule and contains two female gametes: the egg cell (EC) and the central cell (CC). During double fertilization, one sperm fuses with the EC and the other with the CC (2). The fertilized EC develops into the embryo, whereas the fertilized CC forms the endosperm, a placenta-like tissue sustaining embryonic growth (3).

Male and female gametes are in a quiescent state, which ensures that they do not divide in the absence of fertilization and mediates synchronization of their cell cycles when their nuclei fuse upon fertilization. In plants, depending on the species, sperm are arrested in the G₁ (4–10) or G₂ phase (11, 12), whereas it is unclear at which cell cycle stage the female gametes are arrested (10–14).

More than 100 factors govern cell cycle arrest and progression (15, 16), and their deregulation often leads to reduced fertility because of aberrant gametogenesis and/or embryogenesis (17–21). In the model plant *Arabidopsis*, mutations in some cell cycle genes affect only the CC: some cause proliferation in the absence of fertilization, whereas others cause a lack of division upon nuclear fusion (22–26). These observations have fueled the hypothesis that a mechanism preventing cell division operates in the CC, which is lifted by a fertilization-dependent signal (13, 27, 28).

Institute of Plant and Microbial Biology and Zurich-Basel Plant Science Center, University of Zurich, CH-8008 Zurich, Switzerland.

*Corresponding author. Email: grossnik@botinst.uzh.ch (U.G.); sara.simonini@botinst.uzh.ch (S.S.)

would be expected if they were at the same cell cycle stage (fig. S1, E and F). From these two independent analyses, we conclude that before fertilization, the EC is in G₂ phase, whereas the CC has entered but not completed S phase.

The fact that the CC did enter but not complete S phase suggested that DNA replication would resume upon fertilization. To test this hypothesis, we incubated inflorescences of *Arabidopsis* with the nucleotide analog 5-ethynyl-2'-deoxyuridine (EdU) to visualize DNA synthesis in situ before fertilization and at 4, 6, and 8 HAP (Fig. 1, G to I, and fig. S1G). The unfertilized CC incorporated no EdU, indicating the absence of DNA synthesis (Fig. II). This observation was supported by the presence, in the EC and CC, of transcripts encoding the replication licensing factor CTD1a, correlating with the absence of DNA synthesis (35, 36) (table S1). We also detected a green fluorescent protein (GFP)-tagged version of CTD1a in immature (Fig. 1J) and unfertilized CCs (Fig. 1, K to N). These data suggest that the unfertilized CC is arrested in S phase at maturity and, unlike the EC, does not reach the G₂ phase (Fig. 1O).

The CC completes S phase after fertilization

After fertilization, we observed changes in the CC. First, the DNA level increased from 2n/3C to about 3n/5C, indicating successful fertilization (Fig. 1F and fig. S1A) and supporting previous observations that sperm has a DNA content of 1n/2C (11). Second, at ~8 HAP, the ploidy/C-value of the fertilized CC had increased to 3n/6C, indicating that it was now in G₂ phase (Fig. 1F and fig. S1A) and thus that DNA synthesis occurred after fertilization. Third, in some ovules, the EC had a ploidy/C-value of 2n/4C, whereas that of the CC remained 2n/3C (fig. S1A). This was consistent with nonsynchronous nuclear fusion (karyogamy) in ECs and CCs (28, 37–40) and indicates that sperm delivery to the female gametophyte is insufficient to trigger cell cycle reactivation in the CC. Rather, karyogamy is required, because an increase in the ploidy/C-value occurred only in CCs with a ploidy/C-value of 3n/5C. Consistent with this increase in the ploidy/C-value, we also observed EdU staining, indicative of active DNA synthesis, specifically in the CCs of fertilized ovules (Fig. 1, H and I), and depletion of CTD1a-GFP, typically occurring when the S phase is initiated, exclusively in the CC (Fig. 1, L to N). The EC behaved very differently upon fertilization: its ploidy/C-value increased from 1n/2C to 2n/4C (Fig. 1F and fig. S1A) without detectable EdU incorporation (Fig. 1I) or persistent CTD1a-GFP fluorescence (Fig. 1, K to N). These observations confirm that mature ECs and sperm cells are arrested in G₂ phase (11) and reveal that replication of the CC genome is completed only after karyogamy (Fig. 1O).

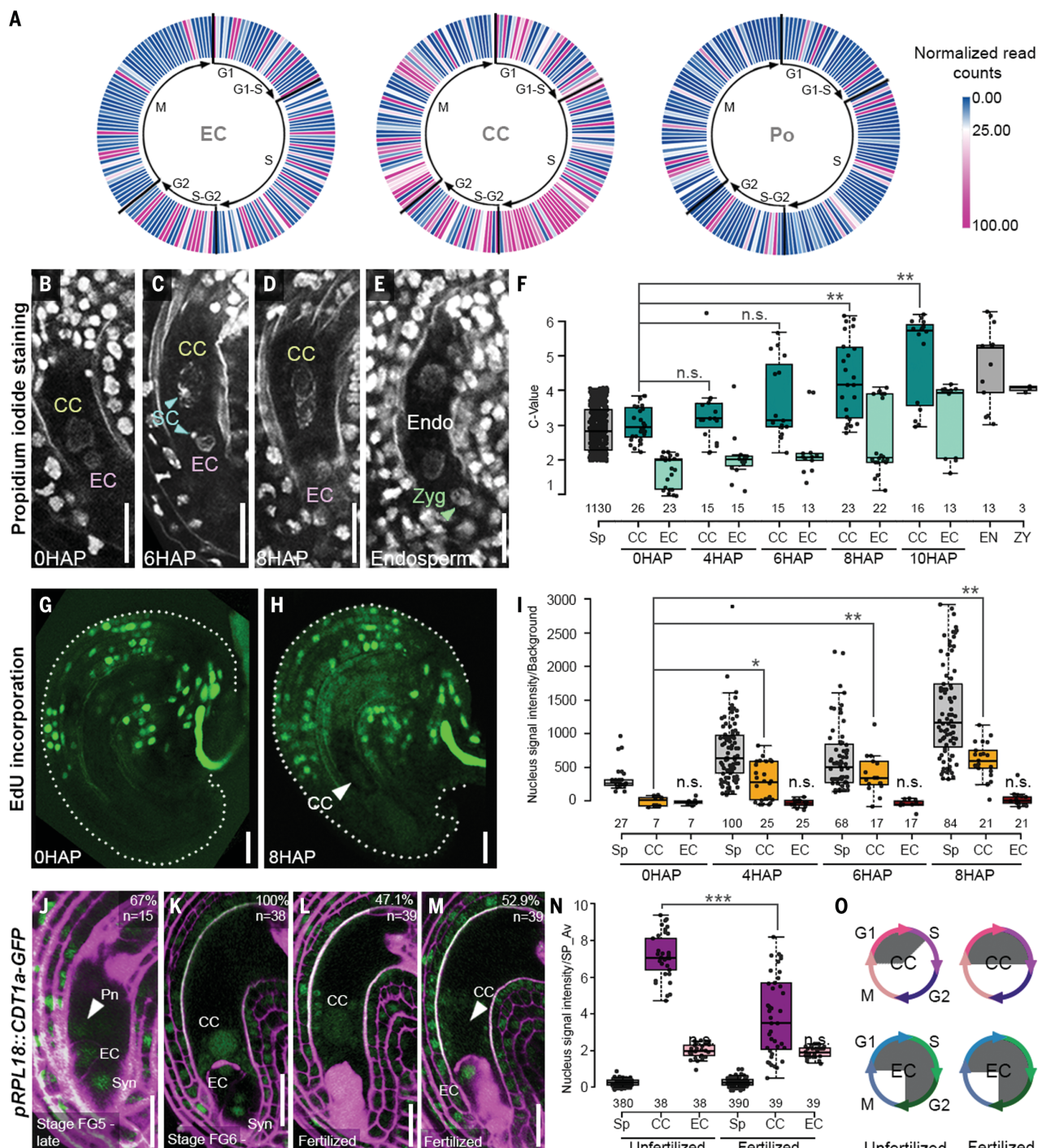


Fig. 1. Quiescent ECs are in the G₂ phase of the cell cycle and CCs arrest in S phase, which is completed only upon fertilization. (A) Circular heatmap of the relative expression levels of transcripts encoding cell cycle components in the EC, CC, and pollen (PO). Genes are organized according to their expression at the different phases of the cell cycle from G₁ to M, as indicated. A single gene may be represented in more than one phase according to its function. (B to E) Representative images of PI-stained ovules showing the female gametophyte at various times (in HAP), as indicated, and after the first endosperm division. Endo, endosperm; Zyg, zygote; SC, sperm cell. (F) Box plots showing quantification of PI staining, as in (B) to (E), indicating the ploidy/C-values of sporophytic (Sp) cells, CC (dark green), EC (light green), endosperm (EN), and zygote (ZY) at the indicated times (in HAP). (G and H) Representative images of EdU staining of ovules at the indicated time points after pollination. (I) Box plots showing quantification of EdU signals as in (G) and (H) in Sp

cells, CCs (orange), and ECs (red) at the indicated time points (in HAP). (J to M) Confocal fluorescence microscopy analyses of CDT1a-GFP (green) in the female gametophyte before (J) and after (K) fusion of the polar nuclei (Pn) in the CC before fertilization and in the primary endosperm nucleus after fertilization [(L) and (M)]. Cell walls were stained with PI (purple). Fertilized ovules are identified by accumulation of PI in the degenerated synergid cell (Syn). (N) Quantification of CDT1a-GFP signal intensity in the nuclei of Sp cells, ECs (purple), and CCs (pink) in unfertilized and fertilized ovules. Values for each category are normalized to the averaged signal intensity value of 10 Sp cells surrounding the female gametophyte. (O) Schematic representation summarizing the cell cycle phases of the EC and CC relative to fertilization. Unfertilized mature ECs are in G₂ phase, unfertilized CCs are arrested in S phase, and fertilized CCs have completed S phase. Scale bars, 20 μ m. n.s., not significant; *P < 0.01; **P < 0.001; and ***P < 0.0001 according to a t test.

Degradation of RBR1 in the CC is required for cell cycle progression

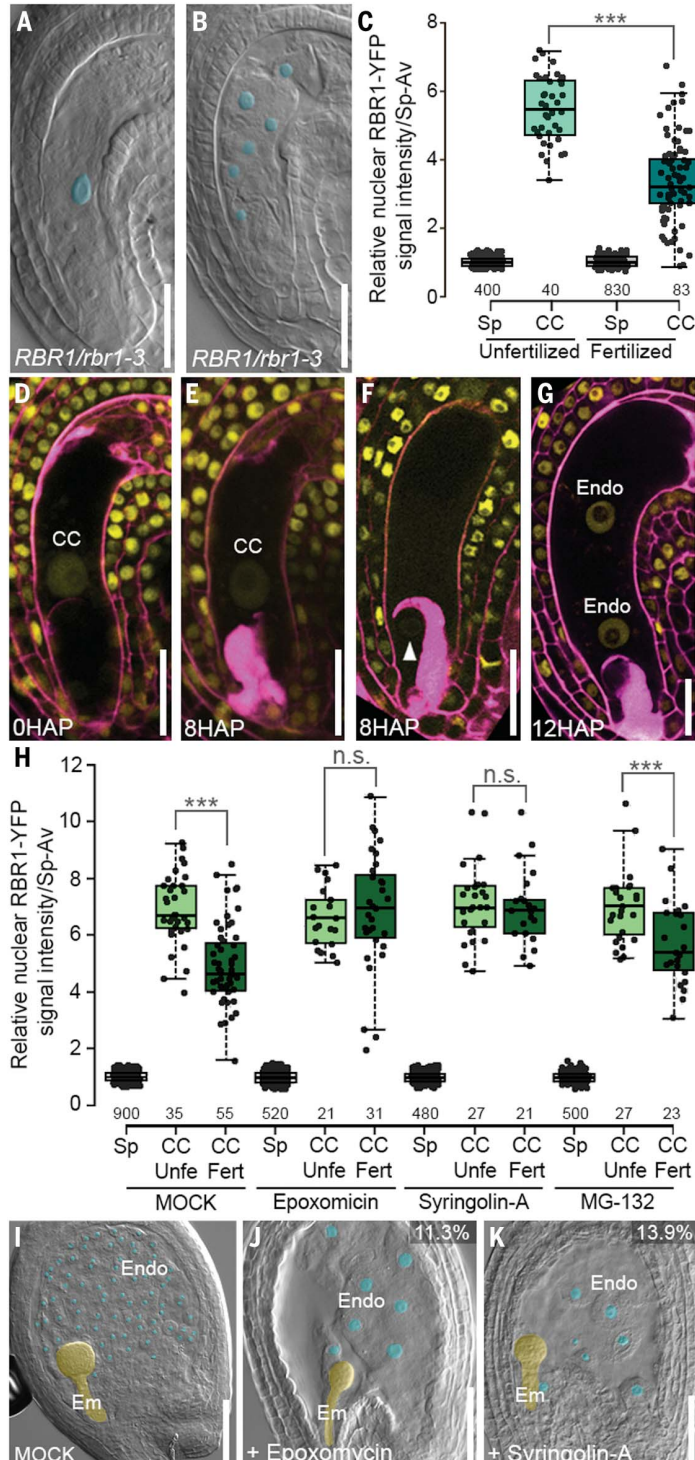
To investigate the mechanism underlying karyogamy-dependent DNA synthesis in the CC, we focused on RETINOBLASTOMA RELATED1 (RBR1) (41–44), an evolutionarily conserved, potent inhibitor of entry into and progression through the S phase (45–47). In *Arabidopsis*, *rbr1* mutant CCs undergo uncontrolled divisions to produce an endosperm-like structure (23) (Fig.

2, A and B), suggesting that RBR1 may be involved in preventing S phase completion in the CC. We investigated RBR1 dynamics in the CC around fertilization by analyzing expression of a yellow fluorescent protein (YFP)-tagged version of the protein, RBR1-YFP (48). Indeed, RBR1 accumulated in unfertilized CCs, as previously described (49) (Fig. 2, C and D). At 7 to 8 HAP, however, CCs exhibited a weaker or undetectable fluorescent signal, before RBR1-

YFP reappeared in both endosperm nuclei after the first division (Fig. 2, C to G).

To determine whether RBR1 degradation in the CC is mediated by the 26S proteasome, as it is in animals and other plant tissues (48, 50), we treated pistils with the 26S proteasome inhibitors epoxomicin, syringolin-A (SylA), and MG-132 and imaged RBR1-YFP around fertilization. When treated with epoxomicin or SylA, the RBR1-YFP signal persisted in the fertilized

Fig. 2. Degradation of RBR1 in the CC is required for cell cycle progression. (A and B) Cleared, unfertilized ovules of *RBR1/rbr1-3* plants showing a wild-type (WT) female gametophyte (A) and a mutant female gametophyte (B), in which the CC has undergone divisions in absence of fertilization. The CC nucleolus (A) and the endosperm-like nucleoli (B) are artificially colored cyan. Scale bars, 20 μ m. (C) Quantification of RBR1-YFP signal intensity in Sp cells and CCs of unfertilized and fertilized ovules. Values for each category are normalized to the averaged signal intensity of 10 Sp cells surrounding the female gametophyte. Scale bars, 20 μ m. (D to G) Representative images of ovules expressing RBR1-YFP (yellow) at various time points (in HAP), as indicated. The contrast of the image in (F) was increased to reveal the faint RBR1-YFP signal in the nucleus of the synergid cell (white arrowhead). Cell walls were stained with PI (purple). Scale bars, 20 μ m. (H) Quantification of RBR1-YFP signal in Sp cells, unfertilized (Unfe) CCs (light green), and fertilized (Fert) CCs (dark green) in inflorescences treated with a mock solution or with the proteasome inhibitors epoxomicin, syringolin-A (Syl-A), and MG-132. Values for each category are normalized to the averaged signal intensity value of 10 Sp cells surrounding the female gametophyte. (I to K) Cleared seeds of inflorescences treated with a mock solution (I), epoxomicin (J), and Syl-A (K). At the top right corner is the percentage of seeds showing the corresponding phenotype. Embryo and endosperm nucleoli are artificially highlighted in yellow and cyan, respectively. Scale bars, 50 μ m. n.s., not significant and *** $P < 0.0001$ according to a *t* test.



CC at ~8 HAP, whereas it disappeared from mock-treated pistils (Fig. 2H), indicating that these inhibitors prevented or slowed down RBR1-YFP degradation in the CC nucleus. Although MG-132 is reported to inhibit RBR1 degradation (48), it had no statistically significant effect on RBR1-YFP stability in our experiments (Fig. 2H). This might be explained by the chemical properties of the inhibitors: MG-132 is a reversible inhibitor that is highly unstable in water, whereas epoxomicin and Syl-A are high-affinity, water-stable, irreversible inhibitors.

We repeated the epoxomicin and Syl-A treatments and left pollinated pistils to develop for another 4 days without inhibitors. A single treatment of ~2 hours led to the formation of seeds with apparently normal, globular-stage embryos that were surrounded by a few, massively enlarged endosperm nuclei (Fig. 2, I to K). Similar endosperm phenotypes were previously observed in plants lacking components of the DNA replication machinery (25–27) or CULLIN4 (51), an E3 ubiquitin-ligase involved in protein degradation by the 26S proteasome. The similarities between the phenotype of these mutants and our inhibitor treatments support the conclusion that protein degradation and DNA synthesis are required for normal endosperm development.

CCs express several CYCLIN-DEPENDENT KINASES (CDKs) (19) that, by dimerizing with cyclins, phosphorylate RBR1 and provoke its degradation (fig. S2, A to E). To prevent RBR1 degradation before fertilization, the CC is equipped with KIP-RELATED PROTEINS (KRPs) that bind to CDKs and inhibit their function. In *ick1,2,6,7* mutant plants, which lack four KRPs (52), we observed that 13.1% of unfertilized ovules contained two to four endosperm-like nuclei, indicating division of the CC in the absence of fertilization (fig. S2, A to D). Together with the data described above (fig. S2E), this indicates that RBR1 persistence in the CC results in cell cycle arrest, preventing progression to the G₂ phase. Moreover, RBR1 degradation is a prerequisite for S phase completion, ultimately ensuring that synchronized maternal and paternal genomes initiate proper endosperm development.

Sperm cell cycle components are delivered to the female gametes upon fertilization

To understand how RBR1 degradation is induced upon fertilization in the CC, we isolated CCs by laser-assisted microdissection at various time points after pollination and analyzed their transcriptomes (Fig. 3A; table S2; and fig. S3, A to D). RBR1 protein degradation in the fertilized CC occurs at ~8 HAP (Fig. 2, C to G). We therefore searched for transcripts that were the most abundant at this time. Such a peak in abundance might be caused by fertilization-dependent de novo transcription or by delivery of paternal transcripts from the sperm to the

CC upon gamete fusion. Because RBR1 degradation occurs through a cell cycle-regulated mechanism (45, 53–55), we focused on transcripts encoding cell cycle components (Fig. 3B). Transcripts of the *CYCD7;1* gene, encoding a cyclin D-type family member, were absent from unfertilized CCs but highly abundant at 8 HAP. D-type cyclins mediate entry into the S phase (56, 57). *CYCD7;1* interacts with RBR1 and promotes its degradation (58, 59) and is the only D-type cyclin that is highly expressed in pollen (31, 58). Moreover, ectopic expression of *CYCD7;1* induces CC proliferation in the absence of fertilization (60). We thus hypothesized that *CYCD7;1* is a paternal signal that is stored in the sperm and delivered to the CC upon fertilization, thus provoking RBR1 degradation and S phase completion.

To test whether *CYCD7;1* is a paternal signal, we looked for *CYCD7;1* mRNA in sperm and unfertilized ovules by *in situ* hybridization on WT ovules fertilized with pollen expressing a *pCYCD7;1::CYCD7;1-YFP* transgene (58). A YFP-specific antisense probe (Fig. 3, C to J) allowed us to distinguish maternal and paternal transcripts in fertilized CCs. In *pCYCD7;1::CYCD7;1-YFP* plants, signal was detected during pollen development (Fig. 3D) and in sperm nuclei of mature pollen grains and elongating pollen tubes (Fig. 3, E and F). At ~4 HAP, a punctate signal was observed in WT ovules, indicative of *CYCD7;1-YFP* transcripts in delivered sperm nuclei (Fig. 3H). In some fertilized ovules at 4 HAP, we detected signals confined to the nuclei of CCs after karyogamy (Fig. 3I), whereas at 8 HAP, they were in the cytoplasm of ECs and CCs (Fig. 3J). The presence of paternal *CYCD7;1* transcripts in fertilized female gametes was confirmed in reciprocal crosses between WT and *cycl7;1* mutant plants using a probe specific to the WT *CYCD7;1* allele (fig. S4, E to J).

We then analyzed the expression of a nuclear-localized YFP protein under control of the *pCYCD7;1* promoter (58), allowing us to monitor its spatiotemporal activity. In ovules, no YFP signal was detected in unfertilized or fertilized ECs or in CCs (Fig. 3L). These data indicate that *CYCD7;1* is transcribed in pollen, where its mRNA is stored in the sperm nuclei and delivered to the female gametes upon fertilization.

The *CYCD7;1* protein is present in mature pollen (58, 61), so we wondered whether it is also stored in sperm nuclei and delivered to female gametes. We fertilized WT plants with pollen from *pCYCD7;1::CYCD7;1-YFP* transgenic plants and analyzed *CYCD7;1-YFP* fluorescence. *CYCD7;1-YFP* was detected in sperm nuclei of mature pollen (Fig. 3M), in growing pollen tubes (Fig. 3N), and in fertilized EC and CC nuclei (Fig. 3, O and P). These data demonstrate that *CYCD7;1* is a paternally derived factor, with both transcripts and proteins being delivered to the female gametes. The restricted

nuclear localization of mRNA and protein likely ensures that *CYCD7;1* is active only upon successful karyogamy and not simply after sperm delivery.

Paternal *CYCD7;1* promotes cell cycle progression of the CC

To investigate whether *CYCD7;1* promotes RBR1 degradation in the CC, we studied the dynamics of RBR1 degradation upon pollination by crossing *pRBR1::mCherry-RBR1* plants (62) with *pCYCD7;1::CYCD7;1-YFP* pollen. We found that RBR1 depletion in the CC occurred after *CYCD7;1* delivery (fig. S4, A to C), consistent with the notion that *CYCD7;1* promotes RBR1 degradation. Moreover, CC-specific (Fig. 4, A and B) or ubiquitous (Fig. 4C) ectopic expression of *CYCD7;1* induced the development of endosperm-like structures in unfertilized ovules, consistent with a previous report (60). The interaction between RBR1 and *CYCD7;1*, which is required for phosphorylation and thus degradation of RBR1, is mediated by a Leu-x-Cys-x-Glu (LxCxE) motif (59, 63). To determine whether this interaction is necessary for RBR1 degradation, we ubiquitously expressed a *CYCD7;1* LxCxE mutant variant (*pRPL18::CYCD7;1^{mut}*) and found that it did not induce CC proliferation in unfertilized ovules (Fig. 4, A to D), indicating that the *CYCD7;1*-RBR1 interaction is required for the S phase to proceed in the CC upon fertilization.

In plants expressing RBR1-YFP and *CYCD7;1* in unfertilized CCs (*pMEA::CYCD7;1*), the RBR1-YFP signal was very weak or undetectable, and endosperm-like structures formed (Fig. 4, E and F). These findings indicate that *CYCD7;1* alone is sufficient to induce RBR1 degradation in the CC and, consequently, to stimulate endosperm proliferation.

To investigate whether *CYCD7;1* exerts paternal control over cell division in fertilized CCs, we used the T-DNA insertion mutants *cycl7;1-1* (58), *cycl7;1-2* (58), and *cycl7;1-3* and a new mutant allele created by CRISPR-Cas9, *cycl7;1^{CRISPR}* (fig. S4D), in reciprocal crosses with WT plants. If paternal delivery of *CYCD7;1* were required for S phase completion in the CC, then its absence would delay division only when *cycl7;1* mutants were used as a male parent, but not as a female parent, in these crosses. We scored the percentage of fertilized ovules with undivided CCs (Fig. 4G) or two, four, or eight endosperm nuclei (Fig. 4, H to J). In crosses of the WT with *cycl7;1* mutant pollen, we observed a significant delay in the first CC division (Fig. 4L and fig. S4E). At 10 HAP, <5% of fertilized ovules in crosses between the WT and *cycl7;1* mutant pollen contained two endosperm nuclei, compared with 30% in crosses between two WT plants (Fig. 4L and fig. S4E). WT and *cycl7;1* mutant pollen tubes grew at similar rates (fig. S5A), indicating that delayed endosperm initiation was not caused

by delayed fertilization. The endosperm of seeds that had received a paternal *cycd7;1* mutant allele started to proliferate at ~16 HAP (Fig. 4L), suggesting that other D-type cyclins might compensate for the absence of CYCD7;1. To investigate this possibility, we created a quadruple *cycd* mutant: *cycd3;1 cycd3;2 cycd3;3 cycd7;1* (*cycd4D*; fig. S5, B and C). When crossing the WT with *cycd4D* pollen, the first endosperm division was even more delayed than in crosses with *cycd7;1* single mutants (99% of ovules at 10 HAP had an undivided CC; Fig. 4L), consistent with other D-type cyclins compensating for the absence of CYCD7;1. Embryo development was unaffected, but we observed several fertilized ovules with undivided CC nuclei next to elongating zygotes (Fig. 4K). Moreover, the delay in initiating endosperm division was exacerbated

when *cycd4D* females were pollinated with *cycd4D* pollen (Fig. 4M). This suggests that the CC becomes transcriptionally active soon after fertilization, producing cell cycle components including D-type cyclins. Early activation of maternal CYCD7;1 was also observed in zygotes (64). Consistent with this conclusion, we detected a YFP signal in plants carrying a maternal *pCYCD7;1::YFP-YFPnls* allele in endosperm containing four nuclei (Fig. 4N), indicating activation of CYCD7;1 transcription at ~20 HAP.

To demonstrate a causal effect between CYCD7;1 delivery by the sperm and RBR1 degradation, we crossed plants expressing RBR1-YFP with WT, *cycd7;1*, or *cycd4D* pollen and analyzed fluorescence after fertilization. RBR1-YFP fluorescence was depleted from

fertilized CCs at ~8 HAP only when WT pollen was used, whereas the RBR1-YFP signal persisted in CCs fertilized with *cycd7;1* or *cycd4D* sperm (Fig. 4O). Stability of RBR1-YFP fluorescence was associated with a lack of DNA synthesis upon fertilization. CCs fertilized by *cycd7;1* or *cycd4D* sperm failed to reach the G₂ phase after fertilization; their ploidy/C values remained at ~3n/5C at 8 HAP, when all CCs fertilized by WT sperm had reached the 3n/6C value (Fig. 4P). We conclude that RBR1 depletion in the CC fails to occur at fertilization in the absence of paternal CYCD7;1 delivery, thereby delaying completion of S phase and progression to G₂ phase.

Discussion

We describe a mechanism ensuring that reactivation of the cell cycle in the CC occurs

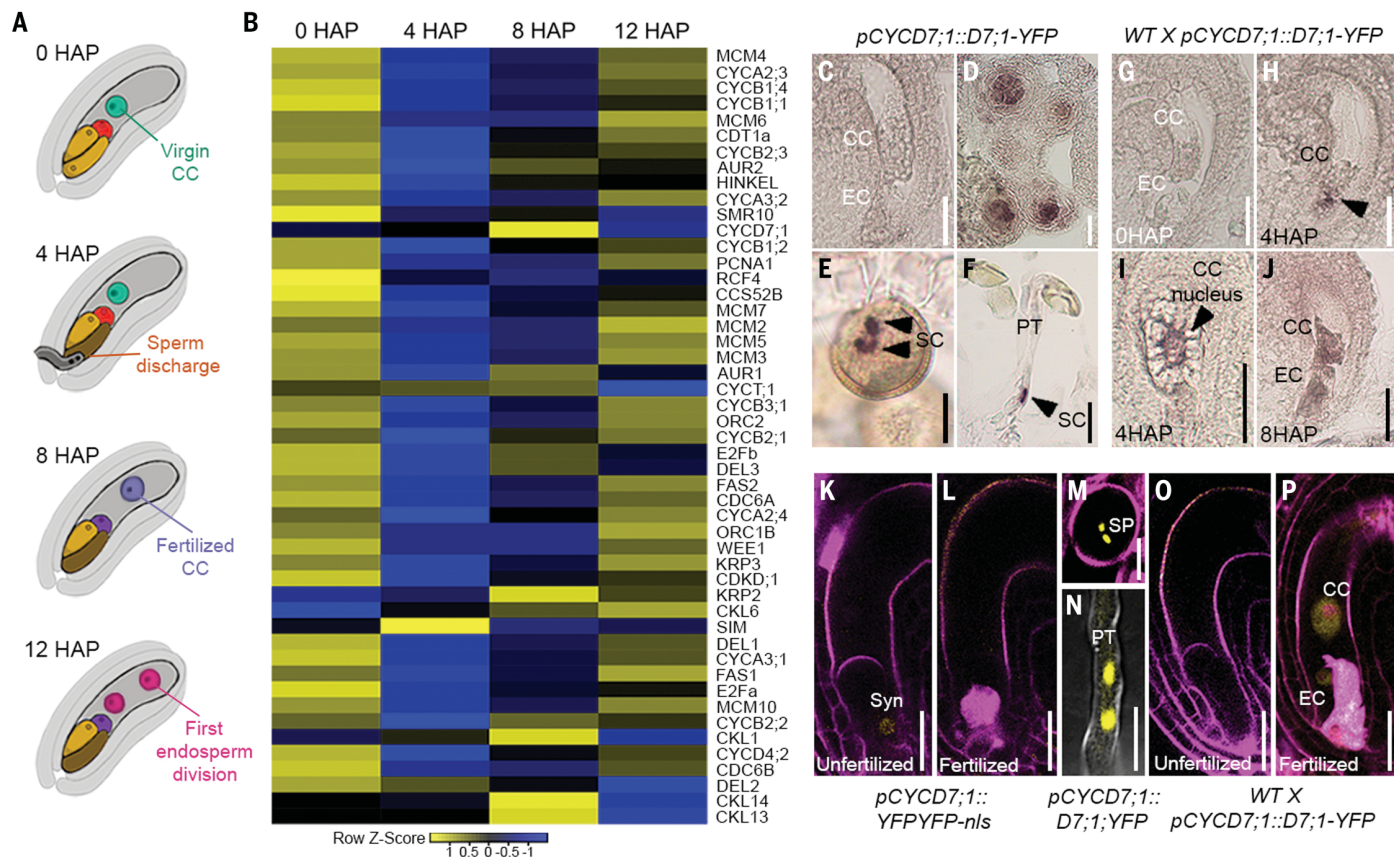


Fig. 3. Paternal CYCD7;1 mRNA and protein are delivered by the sperm cell to the female gametes upon fertilization. (A) Schematic of unfertilized and fertilized female gametophytes used for laser-assisted microdissection of the CC or endosperm. Laser-isolated cell sections were used for transcriptome analysis of the CC at various time points (in HAP), as indicated. Key developmental events and cells (synergid cells: yellow; degenerated synergid cell: brown; unfertilized EC: red; fertilized EC: purple; unfertilized CC: cyan; fertilized CC: blue; endosperm nuclei: pink) are indicated. (B) Heatmap of cell cycle–related genes (right) with transcript levels that vary across the four time points indicated. (C to F) In situ hybridization with a YFP antisense probe on tissues of *pCYCD7;1::CYCD7;1-YFP* (abbreviated as *pCYCD7;1::D7;1-YFP* in the figure) plants showing no signal in unfertilized ovules (C), but a positive signal in anthers (D), and the nuclei of sperm cells (SC, arrowheads) in mature pollen grains (E) and growing pollen tubes

(F). (G and H) In situ hybridization with a YFP antisense probe on WT pistils pollinated with *pCYCD7;1::CYCD7;1-YFP* pollen at the indicated time points (in HAP), showing a signal in the discharged SCs ([H], arrowhead), the CC nucleus ([I], arrowhead), and the nuclei and cytosol of ECs and CCs (J). (K and L) Confocal fluorescence microscopy of YFP-YFPnls driven by the *pCYCD7;1* promoter in unfertilized (K) and fertilized (L) ovules shows no YFP signal in ECs and CCs. Cell walls were stained with PI (purple). (M and N) Confocal fluorescence microscopy of mature pollen grains (M) and pollen tubes (PT) (N) of a *pCYCD7;1::CYCD7;1-YFP* plant showing CYCD7;1-YFP in SC nuclei. Pollen grain cell walls were stained with PI (purple). (O and P) Confocal fluorescence microscopy of unfertilized (O) and fertilized (P) WT ovules pollinated with *pCYCD7;1::CYCD7;1-YFP* pollen showing CYCD7;1-YFP in the fertilized CC and EC. Cell walls were stained with PI (purple). Scale bars in (E), (L), and (N), 10 μm; scale bars in (C), (D), (F) to (K), (M), (O), and (P), 20 μm.

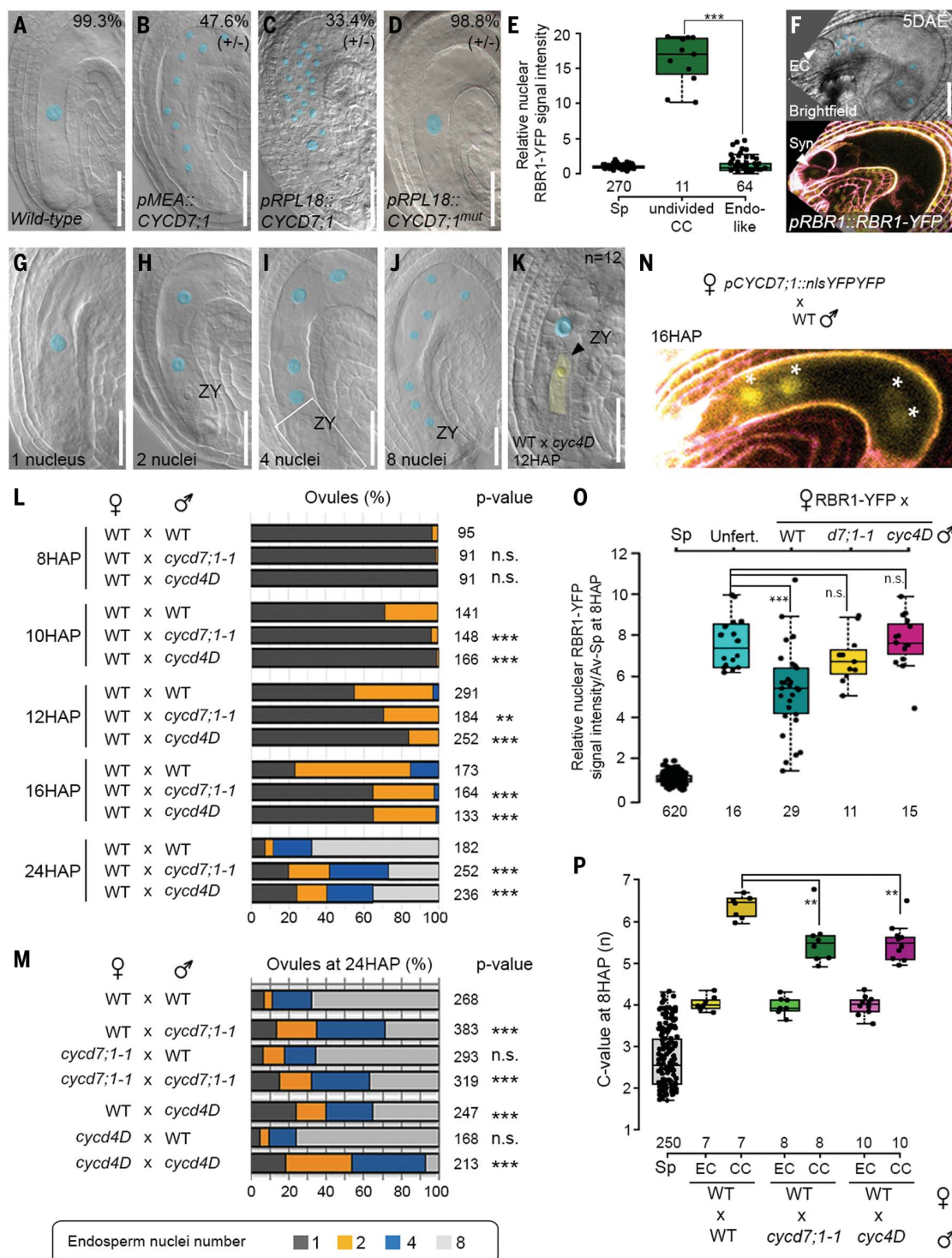


Fig. 4. Paternally derived CYCD7;1 promotes cell cycle progression and RBR1 degradation in the CC. (A and B) Cleared ovules of WT and hemizygous *pMEA::CYCD7;1*- plants with CC-specific expression of *CYCD7;1* showing a WT-looking ovule with an undivided CC (A) and an ovule in which the CC has proliferated ($n = 28$ of 30 independent transformants). The percentage of ovules with the corresponding phenotype is indicated in the top right corner. Endosperm-like nucleoli (C) and the CC nucleolus (D) are artificially colored cyan. (C and D) Cleared ovules of hemizygous *pRPL18::CYCD7;1*- and *pRPL18::CYCD7;1^{mut}*- plants with ubiquitous expression of *CYCD7;1* and *CYCD7;1^{mut}*, respectively, showing an ovule in which the CC has proliferated [$n = 18$ of 26 independent transformants (C)] and a WT-looking ovule (D). The percentage of ovules with the corresponding phenotype is indicated in the top right corner. Endosperm-like nucleoli (C) and the CC nucleolus (D) are artificially colored cyan. (E) Quantification of the RBR1-YFP signal in undivided CCs and endosperm-like nuclei of hemizygous *pMEA::CYCD7;1*- plants 5 days after emasculation (DAE). For each ovule showing CC proliferation, four representative nuclei were selected for quantification. (F) Example of the RBR1-YFP signal (bottom) in an ovule of a hemizygous *pMEA::CYCD7;1*- plant showing CC proliferation in the absence of fertilization (top). Endosperm-like nucleoli are artificially colored cyan. Syn, synergid cells. (G to J) Cleared fertilized ovules showing four stages of

transformants (G) and a WT-looking ovule (D). The percentage of ovules with the corresponding phenotype is indicated in the top right corner. Endosperm-like nucleoli (C) and the CC nucleolus (D) are artificially colored cyan. (E) Quantification of the RBR1-YFP signal in undivided CCs and endosperm-like nuclei of hemizygous *pMEA::CYCD7;1*- plants 5 days after emasculation (DAE). For each ovule showing CC proliferation, four representative nuclei were selected for quantification. (F) Example of the RBR1-YFP signal (bottom) in an ovule of a hemizygous *pMEA::CYCD7;1*- plant showing CC proliferation in the absence of fertilization (top). Endosperm-like nucleoli are artificially colored cyan. Syn, synergid cells. (G to J) Cleared fertilized ovules showing four stages of

endosperm development: fertilized CC (G) and two (H), four (I), and eight (J) endosperm nuclei. The CC nucleolus and endosperm-like nucleoli are artificially colored cyan. ZY, zygote. (K) Cleared WT ovule fertilized with *cycd4D* pollen at 12 HAP showing an undivided CC nucleus (artificially colored cyan) next to the elongating ZY artificially colored yellow. (L) Classification of fertilized ovules (%) based on the number of endosperm nuclei at the indicated time points (in HAP) in crosses between WT × WT, WT × *cycd7;1*, and WT × *cyc4D* plants. Sample size is indicated on the right side of each bar. The color key is indicated at the bottom of panel (M). The P value was calculated using a chi-square test with Egon Pearson correction where appropriate. (M) Classification of fertilized ovules (%) based on the number of endosperm nuclei at 24 HAP in reciprocal crosses between WT, *cycd7;1*, and *cyc4D* individuals. Sample size is indicated on the

right side of each bar. The color key is indicated at the bottom. The P value was calculated using a chi-square test with Egon Pearson correction where appropriate. (N) Confocal fluorescence microscopy of ovules derived from a cross of a *pCYCD7;1::YFPYFPnls* female with WT pollen at 16 HAP showing activation of the maternal *pCYCD7;1::YFPYFPnls* transgene. Asterisks mark endosperm nuclei with a YFPYFPnls signal. (O) Box plots showing quantification of RBR1-YFP signal in unfertilized CCs and in CCs of pistils pollinated with WT, *cycd7;1*, or *cyc4D* pollen. n.s., not significant; **P < 0.001; and ***P < 0.0001 according to a t test. (P) Quantification of ploidy/C-values by PI staining of CCs and ECs of WT pistils pollinated with WT, *cycd7;1*, or *cyc4D* pollen at 8 HAP. n.s., not significant; ***P < 0.001; and ***P < 0.0001 according to a t test. Scale bars, 20 μm.

precisely upon fertilization. We propose that, upon delivery of CYCD7;1 by the sperm, an active CDK-CYCD7;1 complex forms and initiates RBR1 degradation (fig. S6A). Several CDKs are highly expressed in the CC (19) and are known to be important for endosperm development (19, 65), but RBR1 is not degraded before fertilization. This is likely because there are no D-type cyclins to activate CDKs before their delivery by the sperm, but also because several KRP s are present that inhibit CDK function.

The observation that the quiescent CC is arrested in S phase is unusual and opens new questions. S phase is typically arrested when the DNA integrity checkpoint has not been satisfied, e.g., because of DNA damage, but also upon oxidative stress or depletion of nucleotides. Upon DNA damage, pRB, the animal homolog of RBR1, localizes to replication origins, arresting DNA synthesis and inhibiting S phase progression by attenuating cyclin and Cdk activity (47, 66–68). The replication licensing factor CDT1, which usually gets degraded upon S phase entry, also accumulates on damaged chromatin (69). Thus, in addition to their canonical activity at the G₁-to-S transition, animal pRB and CTD1 function during S phase arrest, consistent with our observations in the *Arabidopsis* CC.

We can only speculate about the cause of S phase arrest in the CC. Consistent with the findings in animals mentioned above, the CC nucleus may experience either DNA damage caused by extensive DNA demethylation occurring before fertilization (70) or oxidative stress (71). Consistent with the latter, oxidative stress-related genes are highly enriched among genes changing expression in the CC upon fertilization (fig. S6B).

Paternal CYCD7;1-dependent RBR1 degradation seems specific to the CC because the fertilized EC does not rely on paternal CYCD7;1 to initiate the first division. This is as expected because a cell in G₂ phase does not require DNA synthesis regulated by RBR1 degradation for cell cycle progression. Our findings suggests that the EC and CC, although genetically identical, use different pathways to integrate cell cycle progression with developmental programs that may rely on regulating a component's activity rather than its expression, as we showed for RBR1.

Previously, only two factors were known to be required specifically in one female gamete. The *SHORT SUSPENSOR* transcript accumulates in sperm and is delivered to the female gametes, where it controls development of the embryonic suspensor (72), and peptides encoded by the *EMBRYO SURROUNDING FACTOR1* gene family accumulate in the CC and nonautonomously control suspensor development (73). By contrast, CYCD7;1 is a paternal, sperm-derived signal that specifically controls CC proliferation and thus endosperm formation.

Our findings provide insights into how a cell determines when it is time to divide, a question that is of particular relevance to female gametes because embryogenesis or endosperm development fail if division occurs before fertilization. Given the conserved roles of the factors involved, understanding the fertilization-dependent molecular mechanisms that control endosperm initiation might help in the design of strategies to manipulate seed development in crops.

REFERENCES AND NOTES

1. H. Sawada, N. Inoue, M. Iwano, in *Sexual Reproduction in Animals and Plants*, (Springer, 2014); <https://link.springer.com/book/10.1007/978-4-431-54589-7>.
2. G. N. Drews, A. M. G. Koltunow, in *The Arabidopsis Book* (ASPB, 2011), vol. 2011; <https://doi.org/10.1199/tab.0155>.
3. F. Berger, *Curr. Opin. Plant Biol.* **6**, 42–50 (2003).
4. Y. Matsuda, T. Saito, M. Koseki, T. Z. Shimada, *Plant Physiol.* **9**, 1–6 (1990).
5. L. J. Goff, A. W. Coleman, *Dev. Biol.* **102**, 173–194 (1984).
6. Z. Pónya et al., *Protoplasma* **208**, 163–172 (1999).
7. Y. Sukawa, T. Okamoto, *Plant Reprod.* **31**, 107–116 (2018).
8. H. L. Mogensen, N. Leduc, E. Matthys-Rochon, C. Dumas, *Planta* **197**, 641–645 (1995).
9. H. L. Mogensen, P. B. Holm, *Plant Cell* **7**, 487–494 (1995).
10. X.-Q. Liu et al., *Plant Physiol.* **185**, 137–145 (2021).
11. W. E. Friedman, *Development* **126**, 1065–1075 (1999).
12. H. Q. Tian, T. Yuan, S. D. Russell, *Sex. Plant Reprod.* **17**, 243–252 (2005).
13. F. Berger, Y. Hamamura, M. Ingouff, T. Higashiyama, *Trends Plant Sci.* **13**, 437–443 (2008).
14. J. Chen et al., *Plant Cell* **29**, 2106–2125 (2017).
15. C. Gutierrez, in *The Arabidopsis Book* (ASPB, 2009), vol. 2009; <https://doi.org/10.1199/tab.0120>.
16. M. Malumbres, M. Barbacid, *Nat. Rev. Cancer* **9**, 153–166 (2009).
17. S. Simonini et al., *Dev. Cell* **56**, 1945–1960.e7 (2021).
18. G. J. Campbell, E. L. Hands, M. Van de Pette, *Int. J. Mol. Sci.* **21**, 5343 (2020).
19. M. K. Nowack et al., *Dev. Cell* **22**, 1030–1040 (2012).
20. C. Ebel, L. Mariconti, W. Gruissem, *Nature* **429**, 776–780 (2004).
21. M. Romeiro Motta et al., *EMBO Rep.* **23**, e53995 (2022).
22. L. Borghi et al., *Plant Cell* **22**, 1792–1811 (2010).
23. A. J. Johnston, E. Matveeva, O. Kirilukhova, U. Grossniklaus, W. Gruissem, *Curr. Biol.* **18**, 1680–1686 (2008).
24. D. A. Ni et al., *New Phytol.* **184**, 311–322 (2009).
25. P. S. Springer, D. R. Holding, A. Groover, C. Yordan, R. A. Martienssen, *Development* **127**, 1815–1822 (2000).
26. M. A. Collinge, C. Spillane, C. Köhler, J. Ghyselinck, U. Grossniklaus, *Plant Cell* **16**, 1035–1046 (2004).
27. M. K. Nowack et al., *Nat. Genet.* **38**, 63–67 (2006).
28. S. J. Aw, Y. Hamamura, Z. Chen, A. Schnittger, F. Berger, *Development* **137**, 2683–2690 (2010).
29. M. W. Schmid et al., *PLOS ONE* **7**, e29685 (2012).
30. A. Schmidt et al., *PLOS Biol.* **9**, e1001155 (2011).
31. A. E. Loraine, S. McCormick, A. Estrada, K. Patel, P. Qin, *Plant Physiol.* **162**, 1092–1109 (2013).
32. W. She, D. Grimanelli, C. Baroux, *J. Vis. Exp.* **88**, e51530 (2014).
33. D. Susaki et al., *PLOS Biol.* **19**, e3001123 (2021).
34. S. Adachi et al., *Proc. Natl. Acad. Sci. U.S.A.* **108**, 10004–10009 (2011).
35. B. Desvoyes, A. Arana-Echarri, M. D. Barea, C. Gutierrez, *Nat. Plants* **6**, 1330–1334 (2020).
36. H. Nishitani, S. Taraviras, Z. Lygerou, T. Nishimoto, *J. Biol. Chem.* **276**, 44905–44911 (2001).
37. Y. Hamamura et al., *Nat. Commun.* **5**, 4722 (2014).
38. Y. Hamamura et al., *Curr. Biol.* **21**, 497–502 (2011).
39. M. Ingouff, Y. Hamamura, M. Gourgues, T. Higashiyama, F. Berger, *Curr. Biol.* **17**, 1032–1037 (2007).
40. G. C. Pagnussat et al., *Development* **132**, 603–614 (2005).
41. Q. Xie, A. P. Sanz-Burgos, G. J. Hannon, C. Gutiérrez, *EMBO J.* **15**, 4900–4908 (1996).
42. G. Grafi et al., *Proc. Natl. Acad. Sci. U.S.A.* **93**, 8962–8967 (1996).
43. L. J. Kong et al., *EMBO J.* **19**, 3485–3495 (2000).
44. B. Desvoyes, C. Gutierrez, *EMBO J.* **39**, e105802 (2020).
45. R. A. Weinberg, *Cell* **81**, 323–330 (1995).
46. K. E. Knudsen et al., *Mol. Cell. Biol.* **20**, 7751–7763 (2000).
47. D. Avni et al., *Mol. Cell* **12**, 735–746 (2003).
48. A. Cruz-Ramírez et al., *Cell* **150**, 1002–1015 (2012).
49. P. E. Jullien et al., *PLOS Biol.* **6**, e194 (2008).
50. P. Sdek et al., *Mol. Cell* **20**, 699–708 (2005).
51. E. Dumbliauskas et al., *EMBO J.* **30**, 731–743 (2011).
52. L. Cao et al., *PLOS Genet.* **14**, e1007230 (2018).
53. M. B. Boniotti, C. Gutierrez, *Plant J.* **28**, 341–350 (2001).
54. I. Takahashi, S. Kojima, N. Sakaguchi, C. Umeda-Hara, M. Umeda, *Plant Cell Rep.* **29**, 307–315 (2010).
55. H. Nakagami, K. Kawamura, K. Sugisaka, M. Sekine, A. Shinmyo, *Plant Cell* **14**, 1847–1857 (2002).
56. C. E. Cockcroft, B. G. den Boer, J. M. Healy, J. A. Murray, *Nature* **405**, 575–579 (2000).
57. M. Meijer, J. A. H. Murray, *Plant Mol. Biol.* **43**, 621–633 (2000).
58. A. K. Weimer et al., *Development* **145**, dev160671 (2018).
59. J. L. Matos et al., *eLife* **3**, e03271 (2014).
60. E. Sornay, C. Forzani, M. Forero-Vargas, W. Dewitte, J. A. H. Murray, *Plant J.* **84**, 41–55 (2015).
61. J. Adrián et al., *Dev. Cell* **33**, 107–118 (2015).
62. S. Biedermann et al., *EMBO J.* **36**, 1279–1297 (2017).
63. J. O. Lee, A. A. Russo, N. P. Pavletich, *Nature* **391**, 859–865 (1998).
64. P. Zhao et al., *Dev. Cell* **49**, 882–893.e5 (2019).
65. H. Takatsuka, C. Umeda-Hara, M. Umeda, *Plant J.* **82**, 1004–1017 (2015).
66. E. S. Knudsen, C. Buckmaster, T. T. Chen, J. R. Feramisco, J. Y. Wang, *Genes Dev.* **12**, 2278–2292 (1998).

67. A. Yen, R. Sturgill, *Exp. Cell Res.* **241**, 324–331 (1998).
68. S. P. Angus *et al.*, *Mol. Cell. Biol.* **24**, 5404–5420 (2004).
69. A. Kanellou, N. N. Giakoumakis, A. Panagopoulos, S. C. Tsaniras, Z. Lygerou, *Cancer Res.* **40**, 2449–2456 (2020).
70. T.-F. Hsieh *et al.*, *Science* **324**, 1451–1454 (2009).
71. M. V. Martin, D. F. Fiol, V. Sundaresan, E. J. Zabaleta, G. C. Pagnussat, *Plant Cell* **25**, 1573–1591 (2013).
72. M. Bayer *et al.*, *Science* **323**, 1485–1488 (2009).
73. L. M. Costa *et al.*, *Science* **344**, 168–172 (2014).

ACKNOWLEDGMENTS

We thank B. Scheres (Wageningen University and Research), D. Bergmann (Stanford University), C. Gutierrez (CSIC Centro de Biología Molecular ‘Severo Ochoa’), A. Schnittger (University of Hamburg), D. Kurihara (Nagoya University), H. Wang (University of Saskatchewan), the Nottingham *Arabidopsis* Stock Center, and the *Arabidopsis* Stock Center IJPB-INRAE for providing seeds; Z. Hasenkamp and R. Dudler (University of Zurich) for the gift of Syl-A; M. W. Schmid (MWSchmid GmbH) for analysis, figure preparation, and deposition of the LAM-RNA-Seq data; M. Nowack (VIB-Ghent), C. Gutierrez, B. Desvoyes (CSIC Centro de Biología Molecular ‘Severo Ochoa’), and M. Affolter (Biozentrum, University

of Basel) for helpful discussions or comments on the manuscript; C. Featherstone (Life Science Editors) for professional editorial assistance during manuscript preparation; C. Baroux (University of Zurich) for suggestions on image acquisition; C. Eichenberger, F. Pasquer, A. Bolaños, D. Guthörl, and P. Kopf (University of Zurich) for general laboratory support; and members of the CHERI-T meeting for helpful discussions. **Funding:** This project was supported by the University of Zurich, the European Union’s Horizon 2020 research and innovation program (Marie Skłodowska-Curie grant 798953 to S.B.), and the Swiss National Science Foundation (grant 31003A_179553 to U.G.). **Author contributions:** U.G. conceived, supervised, and raised funding for the project. S.S. conceived, designed, and performed the experiments. S.S. and U.G. analyzed and interpreted the data and wrote the manuscript. S.B. generated the CRISPR-Cas9 mutants and overexpression lines, provided technical support for the LAM RNA-Seq, and commented on the manuscript. **Competing interests:** S.S., S.B., and U.G. are inventors on patent application EP22186785.6 submitted by the University of Zurich covering a method for the induction of autonomous endosperm development. **Data and materials availability:** All data are available in the manuscript or the supplementary materials; the RNA-Seq raw data

have been deposited at the National Center for Biotechnology Information Sequence Read Archive under accession number PRJNA989505. **License information:** Copyright © 2024 the authors, some rights reserved; exclusive licensee American Association for the Advancement of Science. No claim to original US government works. <https://www.science.org/about/science-licenses-journal-article-reuse>. This research was funded in whole or in part by the Swiss National Science Foundation (grant 31003A_179553), a cOAlition S organization. The author will make the Accepted Manuscript (AAM) version available under a CC BY public copyright license.

SUPPLEMENTARY MATERIALS

science.org/doi/10.1126/science.adj4996

Materials and Methods

Figs. S1 to S6

Tables S1 to S3

References (74–85)

MDAR Reproducibility Checklist

Submitted 18 July 2023; accepted 4 January 2024
[10.1126/science.adj4996](https://doi.org/10.1126/science.adj4996)